Electronic Supplementary Material (ESI) for Physical Chemistry Chemical Physics.

Supplementary Data:

Experimental evidences for Quantum Cutting Co-operative Energy Transfer process in Pr^{3+}/Yb^{3+} ions co-doped fluorotellurite glass: Dispute over Energy Transfer mechanism

Sathravada Balaji[*1,2], Debarati Ghosh[1,2], Kaushik Biswas[1,2], Gaurav Gupta[2] and Kalyandurg Annapurna[*1,2]

[1]CSIR - Network of Institute for Solar Energy (NISE), New Delhi, India

[2]GSTS, Glass Division, CSIR-Central Glass and Ceramic Research Institute

196, Raja S. C. Mullick Road, Kolkata – 700 032, India

[*]Corresponding authors: sbalaji@cgcri.res.in, annapurnak@cgcri.res.in

Telephone: +91-33-2483 8079/8082; Fax: +91-33-2473 0957

Figure S1: Solar irradiance spectrum (AM1.5) with c-Si-PV spectral response overlaid with Pr^{3+} absorption and Yb^{3+} emission depicting quantum cutting (QC) mechanism among Pr^{3+}-Yb^{3+} ion pairs.

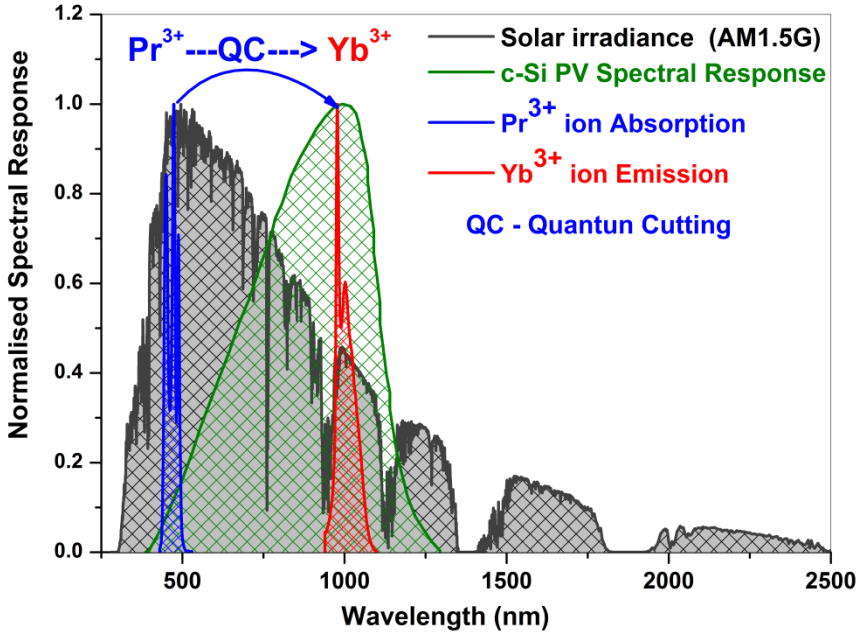

Figure S1 depicts an overview of quantum cutting mechanism how to utilize the thermal energy inducting high energy photons to useful NIR photons in view of c-Si photovoltaic cell.

Figure S2: 'RAMAN' and 'FTIR Reflectance' spectra of TBLAF (Pr0.5) glass

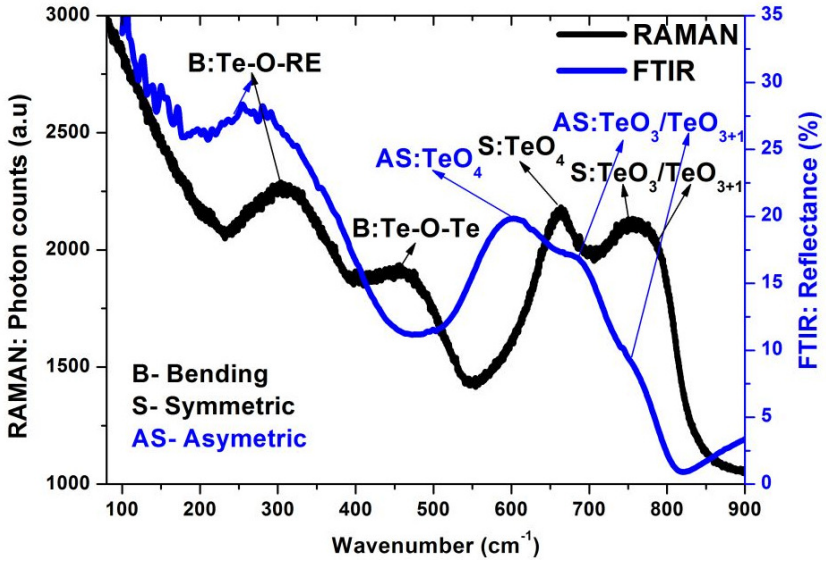

Note: Only for comparison, FTIR-Reflectance and Raman spectra were plotted using double Y-axis scale. The intensities of the bands have their usual meaning as shown in the graph scale.

Figure S2 represents the FTIR relectence spectum (Blue) and Raman (Black) spectrum of the Pr0.5 sample. The Raman active symmetric and FTIR active assymetric vibrations corresponding to the structural units were indicated in the spectrum itself for clear understanding. Raman Spectrum of the glass has been recorded using 486 nm Argon ion laser on confocal Laser Raman Spectrometer (Model: Lab Ram HR 800 EV, HORIBA Jobin Yvon, France). The FTIR reflectance spectrum of the glass sample recorded using a FTIR spectrometer (Model: Frontier, FIR-MIR-FTIR, Perkin-Elmer, USA) at a 15^{o} angle of incidence.

Raman spectrum shows distinct vibrational bands due to symmetric stretching modes of $TeO_4/TeO_3/TeO_{3+1}$in the range 600- 800 cm^{-1}, bending modes due to Te-O-Te at ~450 cm^{-1} and Te-O-RE (RE- Rare Earth element) at ~300 cm^{-1} respectively. FTIR-Reflectance spectrum as shown in the Fig S2 depicts the vibrational bands corresponding to the asymmetric stretching vibrations in the region 480- 800 cm^{-1} and bending vibrations in the range less than 480 cm^{-1}.

The intense peak at ~600 cm^{-1} from FTIR and ~650 cm^{-1} from Raman corresponding to asymmetric and symmetric vibration of main glass forming TeO_4 units respectively indicates the maximum phonon energy of the present glass.

Figure S3: Absorption spectra of only Pr^{3+} (0.5 mol %) doped TBLAF glass.

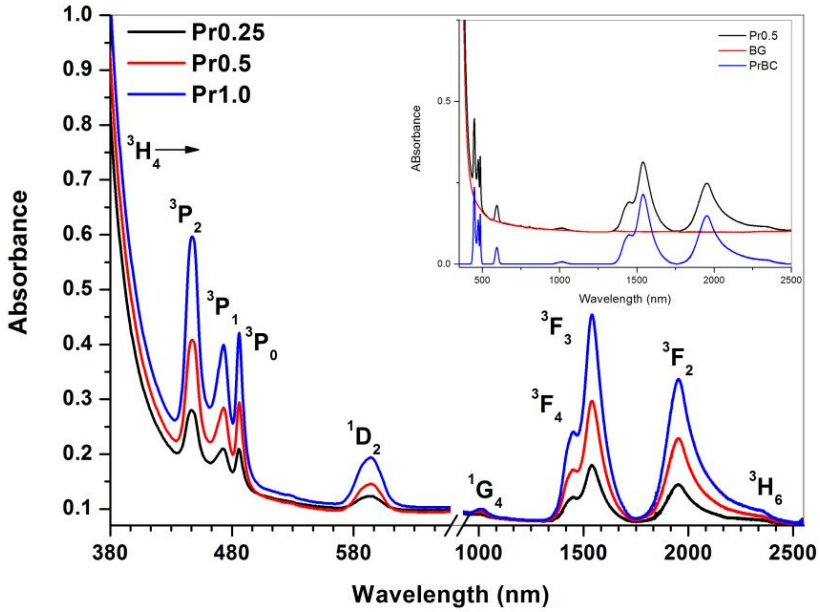

Inset of Figure S3 represents the base glass corrected absorption spectrum for Judd-Oflet analysis.

Judd-Ofelt analysis for Pr^{3+} ions usually produces unsatisfactory results with negative value of J-O intensity parameter, Ω_2. It is often noticed in many hosts when considering the higher energy absorption transitions particularly the hypersensitive (highly host dependent) $^3H_4 \rightarrow {}^3P_2$ transition due to mixing of *4f* and *5d* orbitals. The energy gap between the center gravity of *5d*-electron energies and *4f* electron energies is smallest for Pr^{3+} ions [Ref. 32]. Excluding this $^3H_4 \rightarrow {}^3P_2$ hypersensitive transition in J-O analysis, may result with positive intensity parameter (Ω_2) however, experimentally measured radiative lifetimes and calculated radiative lifetimes differ in big way questioning the reliability of J-O calculated data.

A.A. Kaminskii work [Ref: Phys. Stat. Sol. (B) 157 (1990) 267] on modified J-O theory by including the energy difference of *4f* and *5d* orbitals shown positive values of Ω_2 parameter with good agreement between measured and calculated radiative properties [Ref. 32]. The electric dipole line strength in the modified J-O theory is given as

$$S_{ed} = e^2 \sum_{\lambda=2,4,6} \Omega'_\lambda (1 + 2\alpha(E_J + E_{J'} - 2E_f^0)) \times \langle \psi J \| U^\lambda \| \psi' J' \rangle^2$$

where Ω'_λ are the modified J–O parameters, α is an additional parameter and for Pr^{3+} has a value of about 10^{-5} cm^{-1}. E_J and $E_{J'}$ are the energies of the levels ψJ and ψ'J' respectively, and E_f^0 is the centre of gravity of the *4f* configuration. For Pr^{3+} has a value of 9940 cm^{-1}.

Table S1 presents the Ω_λ intensity parameters were obtained from electric dipole line strength values calculated using modified J-O theory, normal J-O theory where Pr^{3+}: $^3P_2$ state included and not included. Oscillator strength of the respective absorption transition has been calculated from the obtained value of electric dipole (S_{ed}) and magnetic dipole (S_{md}) line strength values. The root mean square deviation from the measured and calculated values is presented in Table S1. RMS values for modified J-O theory are less than $^3P_2$ included normal J-O analysis where as $^3P_2$ not included normal J-O analysis shows low RMS values.

Table S1: Judd-Ofelt Analysis of 0.5 mol % Pr^{3+} doped TBALF glass

Modified Judd-Ofelt Theory						
Transition $^3H_4 \rightarrow$	Wavelength (nm)	$S_{ed}^{mea} \times 10^{20}$	$S_{ed}^{cal} \times 10^{20}$	$P_{mea} \times 10^{6}$	$P_{cal} \times 10^{6}$	Refractive Index 'n'
$^3H_6+^3F_2$	1948	11.236	11.202	13.450	13.408	1.95902
$^3F_3+^3F_4$	1537	14.128	14.388	21.550	21.947	1.96508
$^1G_4$	1013	0.276	0.303	0.653	0.715	1.97902
$^1D_2$	593	1.167	0.616	4.841	2.557	2.02279
$^3P_0$	486	0.912	1.223	4.761	6.382	2.06014
$^3P_1+^1I_6$	472	2.172	1.894	11.747	9.738	2.06749
$^3P_2$	447	3.421	1.472	19.790	8.516	2.08296

$^3H_4 \rightarrow {}^3F_3+{}^3F_4$: $S_{md} = 0.0062 \times 10^{-20}$
$^3H_4 \rightarrow {}^1G_4$: $S_{md} = 0.0021 \times 10^{-20}$

Ω_2 = 11.407×10^{-20}
Ω_4 = 7.076×10^{-20}
Ω_6 = 8.975×10^{-20}

rms $\Delta S_{ed} = \pm1.051\times10^{-20}$
rms $\Delta P = \pm5.898\times10^{-6}$

Normal Judd-Ofelt Theory $^3P_2$ Included

	$S_{ed}^{mea} \times 10^{20}$	$S_{ed}^{cal} \times 10^{20}$	$P_{mea} \times 10^{6}$	$P_{cal} \times 10^{6}$
	7.919	7.875	9.479	9.425
	10.346	10.676	15.784	16.288
	0.221	0.223	0.523	0.526
	1.0963	0.459	4.546	1.905
	0.925	1.309	4.827	6.831
	2.345	1.884	12.054	9.686
	3.592	1.096	20.776	6.337

Ω_2 = 5.917×10^{-20}
Ω_4 = 7.574×10^{-20}
Ω_6 = 6.062×10^{-20}

rms $\Delta S_{ed} = \pm1.333\times10^{-20}$
rms $\Delta P = \pm7.505\times10^{-6}$

Normal Judd-Ofelt Theory $^3P_2$ Not Included

	$S_{ed}^{mea} \times 10^{20}$	$S_{ed}^{cal} \times 10^{20}$	$P_{mea} \times 10^{6}$	$P_{cal} \times 10^{6}$
	7.919	7.923	9.479	9.484
	10.346	10.380	15.784	15.836
	0.221	0.216	0.523	0.510
	1.0963	0.446	4.546	1.850
	0.925	1.325	4.827	6.915
	2.345	1.900	12.054	9.764
	3.592	-	20.776	-

Ω_2 = 6.081×10^{-20}
Ω_4 = 7.667×10^{-20}
Ω_6 = 5.769×10^{-20}

rms $\Delta S_{ed} = \pm0.511\times10^{-20}$
ms $\Delta P = \pm2.054\times10^{-6}$

Radiative properties have been calculated using modified and $^3P_2$ included and not included J-O theory and presented in Table S2. As said earlier, omitting this $^3P_2$ hypersensitive transition (having high oscillator strength) may yield less deviation from measured and calculated oscillator strength values. However, a considerable deviation from measured and calculated radiative rates may be apparent. So, to

validate the J-O theory, the measured lifetime value $^1D_2$ excited state with that of J-O calculated lifetimes have been considered. Since non-radiative relaxation from $^1D_2$ state is considerably negligible (energy difference between $^1D_2$ to $^1G_4$ is ~7135 cm^{-1} which requires almost ~7 phonons to relax in non-radiative way and we know that if the separation between two states exceeds more than 5 phonons then the probability of non-radiative relaxation is negligibly small) and photon emission from this state follows almost radiative path (if not considered impurity centers like OH^- etc.). So the measured lifetime of $^1D_2$ state would be used to validate the goodness of J-O theory.

Table S2: Radiative Properties calculated from J-O analysis

Ems-Trans	*nm*	$^3P_2$ Included			$^3P_2$ Not Included			Modified J-O		
		S_{ed}	A_{rad}	β	S_{ed}	A_{rad}	β	S_{ed}	A_{rad}	β
$^3P_0 \rightarrow {}^1D_2$	2584	7.93E-22	4.852	0.0003	8.15E-22	4.987	0.0003	1.53E-21	9.355	0.0004
$^1G_4$	930	3.22E-21	249.2	0.0134	3.26E-21	252.3	0.0134	3.01E-21	232.9	0.0092
$^3F_4$	731	9.19E-21	1510	0.0814	9.3E-21	1528	0.0812	8.58E-21	1410	0.0556
$^3F_3$	706	0	0	0	0	0	0	0	0	0
$^3F_2$	649	1.74E-20	7634	0.4119	1.79E-20	7846	0.4167	3.36E-20	14718	0.5799
$^3H_6$	616	4.4E-21	865.1	0.0467	4.19E-21	823.3	0.0437	6.52E-21	1281	0.0505
$^3H_5$	544	0	0	0	0	0	0	0	0	0
$^3H_4$	492	1.3E-20	8273	0.4463	1.31E-20	8374	0.4448	1.21E-20	7730	0.3045
$A_{rad} = A_{ed} + A_{md}$ $\tau_{rad} = 1/\Sigma A_{rad}$ $\beta = A_{rad}/\Sigma A_{rad}$				$\Sigma A_{rad}(s^{-1})$= 18536 τ_{rad} (μs)= **53.95**			$\Sigma A_{rad}(s^{-1})$= 18829 τ_{rad} (μs)= **53.11**			$\Sigma A_{rad}(s^{-1})$= 25381 **τ_{rad} (μs)= 39.40**
$^1D_2 \rightarrow {}^1G_4$	1439	3.17E-20	643.3	0.1124	3.22E-20	652.1	0.1132	5.52E-20	1119	0.133
$^3F_4$	1040	3.14E-20	1719	0.3005	3.22E-20	1763	0.3061	6.00E-20	3290	0.3914
$^3F_3$	990	3.05E-21	250.1	0.0437	3.11E-21	255.4	0.0443	4.61E-21	378.4	0.045
$^3F_2$	880	6.94E-21	1256	0.2195	7.04E-21	1273	0.2211	7.25E-21	1313	0.1561
$^3H_6$	810	5.27E-21	434	0.0759	5.31E-21	437.5	0.076	5.11E-21	421.3	0.0501
$^3H_5$	685	1.62E-22	26.78	0.0047	1.63E-22	26.93	0.0047	1.61E-22	26.66	0.0032
$^3H_4$	594	4.36E-21	1392	0.2433	4.23E-21	1352	0.2347	5.82E-21	1860	0.2212
				$\Sigma A_{rad}(s^{-1})$= 5720.9 τ_{rad} (μs)= **174.8**			$\Sigma A_{rad}(s^{-1})$= 5760 **τ_{rad} (μs)= 173.6**			$\Sigma A_{rad}(s^{-1})$= 8408 **τ_{rad} (μs)= 118.9**
$^1G_4 \rightarrow {}^3F_4$	3436	2.91E-20	41.13	0.0431	2.85E-20	40.22	0.043	3.94E-20	55.61	0.041
$^3F_3$	2994	3.13E-21	8.7	0.0091	3E-21	8.352	0.0089	4.57E-21	12.72	0.0094
$^3F_2$	2019	1.25E-21	16.19	0.017	1.25E-21	16.24	0.0174	1.27E-21	16.58	0.0122
$^3H_6$	1855	3.71E-20	240.5	0.2523	3.71E-20	240.1	0.2568	5.22E-20	338	0.2493
$^3H_5$	1373	2.75E-20	526.7	0.5526	2.66E-20	510.2	0.5456	3.86E-20	738.7	0.5448
$^3H_4$	1040	2.17E-21	120	0.1259	2.17E-21	120	0.1283	3.52E-21	194.4	0.1433
S_{md}: **$^1G_4 \rightarrow {}^3H_4$ =** 0.0021×10^{-20}				$\Sigma A_{rad}(s^{-1})$= 953.17 τ_{rad} (ms)= **1.049**			$\Sigma A_{rad}(s^{-1})$= 935.09 **τ_{rad} (ms)= 1.069**			$\Sigma A_{rad}(s^{-1})$= 1356 **τ_{rad} (ms)= 0.737**

Decay time for the $^1D_2$ states have been recorded by monitoring $^1D_2 \rightarrow {}^3F_4$ corresponding to 1040 nm emission (having highest branching ratio of ~39%) upon 588nm excitation as depicted in Figure S4. The decay curves were best fitted to double exponential function. The slower component (t1) describes the decay time of the state which doesn't involved in any quenching process caused by impurity centers or Pr^{3+} ion clusters in contrary to the faster (t2) component.

Figure S4: $^1D_2$ state decay curve of only Pr^{3+} (0.5 mol %) doped TBLAF glasses.

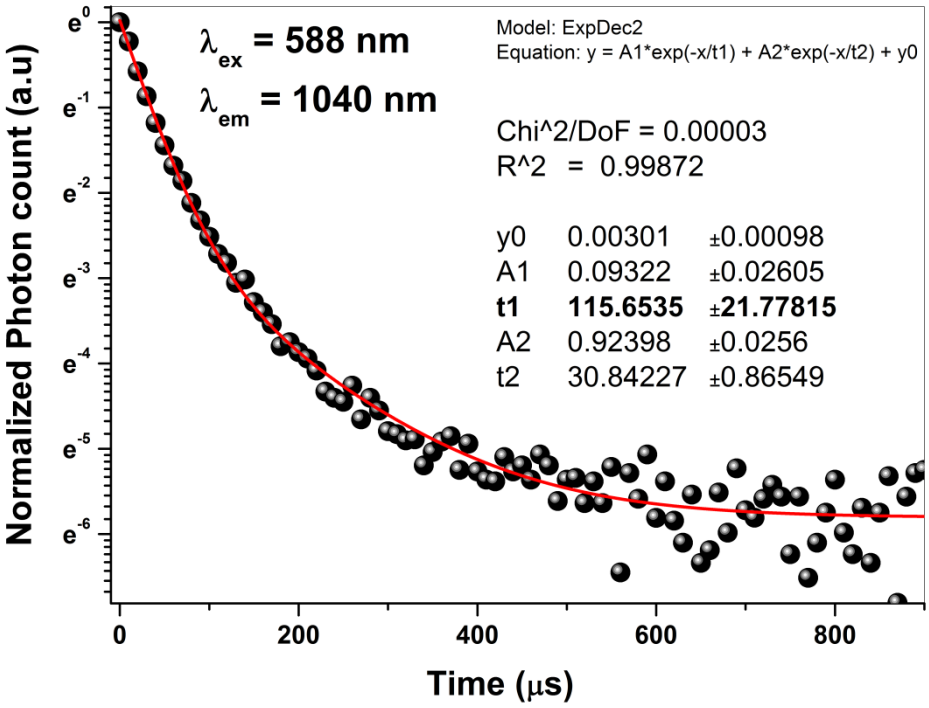

The measured lifetime $^1D_2$ state (115μs ±21.7μs) is in close proximity with that of calculated (118.9μs) lifetime using modified J-O theory suggesting $\Omega_{\lambda=2,4,6}$ intensity parameters derived from modified J-O theory are more valid in the present case compared to the radiative lifetimes calculated using normal J-O theory including and excluding hypersensitive $^3P_2$ transition.

Figure S5: Absorption spectra of only Pr^{3+} (0.5 mol %) doped and Pr^{3+} co-doped with varied Yb^{3+} concentrations in TBLAF glasses.

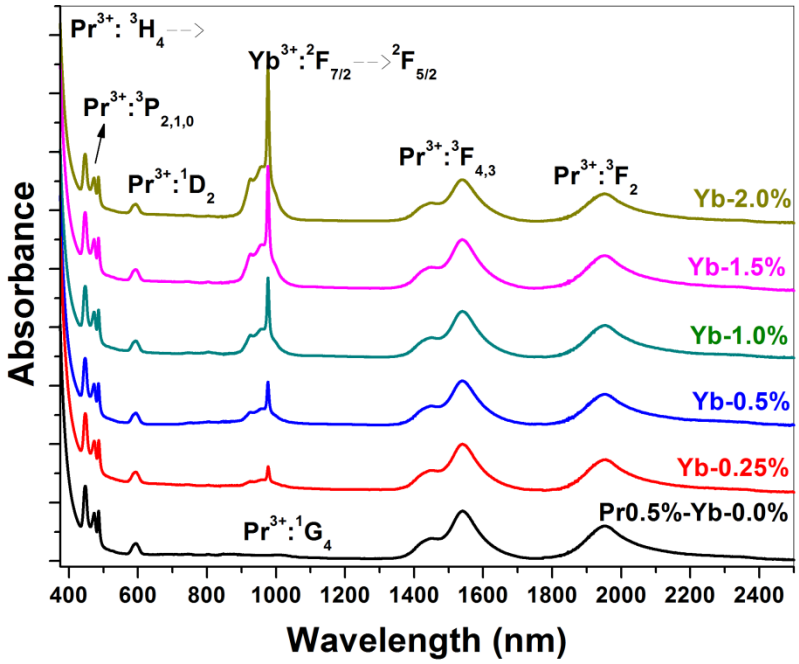

Figure S5 represents the absorption spectra of the glasses containing fixed Pr^{3+} ion and varied Yb^{3+} ion concentrations. The observed bands shows the characteristic absorption transitions of Pr^{3+}: $^3H_4 \rightarrow {}^3P_{2,1,0}$, $^1D_2$, $^3F_{4,3,2}$ at 447 nm, 472 nm, 486 nm, 594 nm, 1014 nm, 1442 nm, 1540 nm, 1953 nm and Yb^{3+}: $^2F_{7/2} \rightarrow {}^2F_{5/2}$ at 977 nm respectively. Apparently, Yb^{3+} ion band intensity increases linearly with increase in Yb^{3+} ion concentration as shown in Fig 5.

Table S3: IH-fitted energy transfer micro parameters; Critical concentration (C_0), Critical distance (R_0), Donor-Acceptor energy transfer micro parameter (C_{DA}), Energy transfer rate (γ^2), Fitting Regression coefficient (R^2)

Sample	C_0 (10^{20} ions/cm^3)	R_0 (Å)	C_{DA} (10^{-37} cm^{6}sec^{-1})	γ^2 (sec^{-1})	R^2
Yb0.25	0.3078	19.794	10.024	176164.88	0.96936
Yb0.5	0.5668	16.149	2.9568	185804.10	0.97766
Yb1.0	1.0112	13.315	0.9289	220712.04	0.98663
Yb1.5	1.4178	11.896	0.4725	248791.46	0.99297
Yb2.0	1.8042	10.978	0.2918	272974.90	0.99480

Figure S6: 447 nm laser power dependent emission spectra

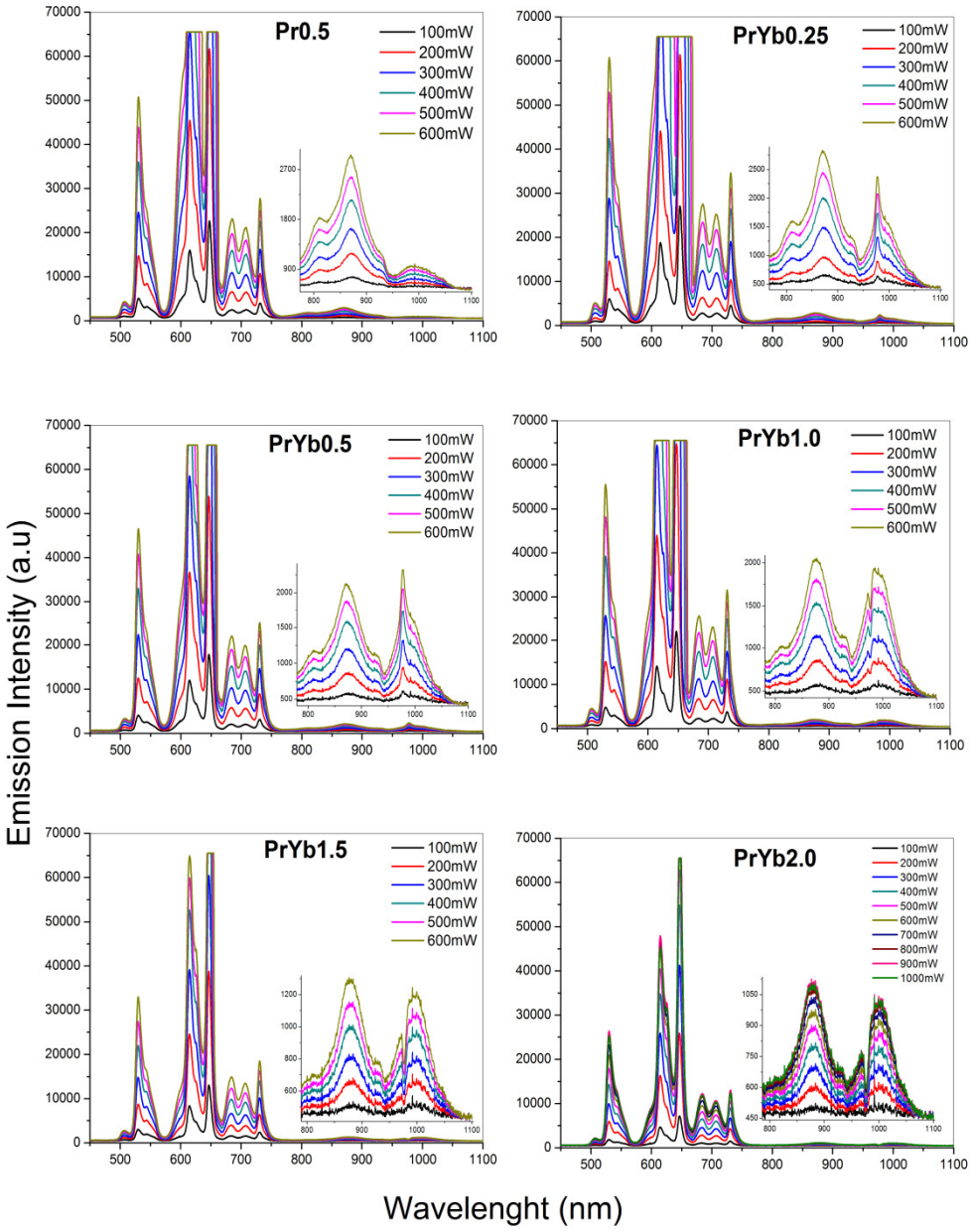

Figure S6 presents the 447 LD power dependent emission spectra for different Yb^{3+} ion concentration. Saturation of Pr^{3+} VIS emission (649 nm) has been observed at higher pump powers. Gradual decrease in the saturation of Pr^{3+} VIS emission on addition of Yb^{3+} ions indicating effectiveness of energy transfer from Pr to Yb. It can also be noticed from the insets of Fig S6 that due to reabsorption of Yb^{3+}: 978 nm emission a sharp dip at ~978 nm has been noticed at higher Yb^{3+} ion concentrations (> 0.5 mol% of Yb^{3+} ions) gradually decreased.